Electronic Supplementary Material (ESI) for Dalton Transactions.

Supporting information

Spin crossover of Fe(II) mononuclear complex induced by intermolecular factors involving chloride and solvent ordering.

Kenneth Zhang,[a†] Matthew J. Wallis,[a†] Alexander R. Craze,[b] Shinya Hayami,[c] Hyunsung Min,[a,d] Daniel J. Fanna,[d] Mohan M Bhadbhade,[e] Ruoming Tian,[e] Christopher E. Marjo,[e] Leonard F. Lindoy[f] and Feng Li*[a]

Author Affiliations

* Corresponding author

† These authors contributed equally to this work

E-mail: Feng.Li@westernsydney.edu.au

a School of Science, Western Sydney University, Locked Bag 1797, Penrith, NSW, Australia

b Department of Chemistry, University of Oxford, Oxford OX1 3TA, United Kingdom

c Department of Chemistry, Graduate School of Science and Technology, Kumamoto University, 2-39-1 Kurokami, Chuo-ku, Japan

d Advanced Materials Characterisation Facility, Western Sydney University, Locked Bag 1797, Penrith, NSW, Australia

e Mark Wainwright Analytical Centre, University of New South Wales, Kensington, NSW, Australia

f School of Chemistry, The University of Sydney, NSW 2006, Australia

Keywords: iron(II), spin crossover, chloride, solvent, mononuclear

Table of Contents

S1. Powder X-ray diffraction measurements

Sample preparation and data processing

Samples of **1** and **2**·6.5H_2O were lightly ground and dry mounted on a low background silicon XRD plate with a thin layer of amorphous grease. Data processing was conducted using Bruker's Eva software. Data refinement of **1** was conducted using CIFs obtained from SCXRD and fitted against the experimental PXRD pattern via the Rietveld refinement method in Bruker's TOPAS v6. The fit of **1** against the experimental powder pattern illustrates that the bulk material is in good agreement with the single crystal structure. Using the **2**-CH_3OH CIF at 300 K, a simulated powder pattern generated by Mercury was overlaid on the experimental powder pattern to demonstrate a difference in powder patterns that suggested a phase change. A CIF of **2**·6.5H_2O was unable to be obtained due to crystal degradation.

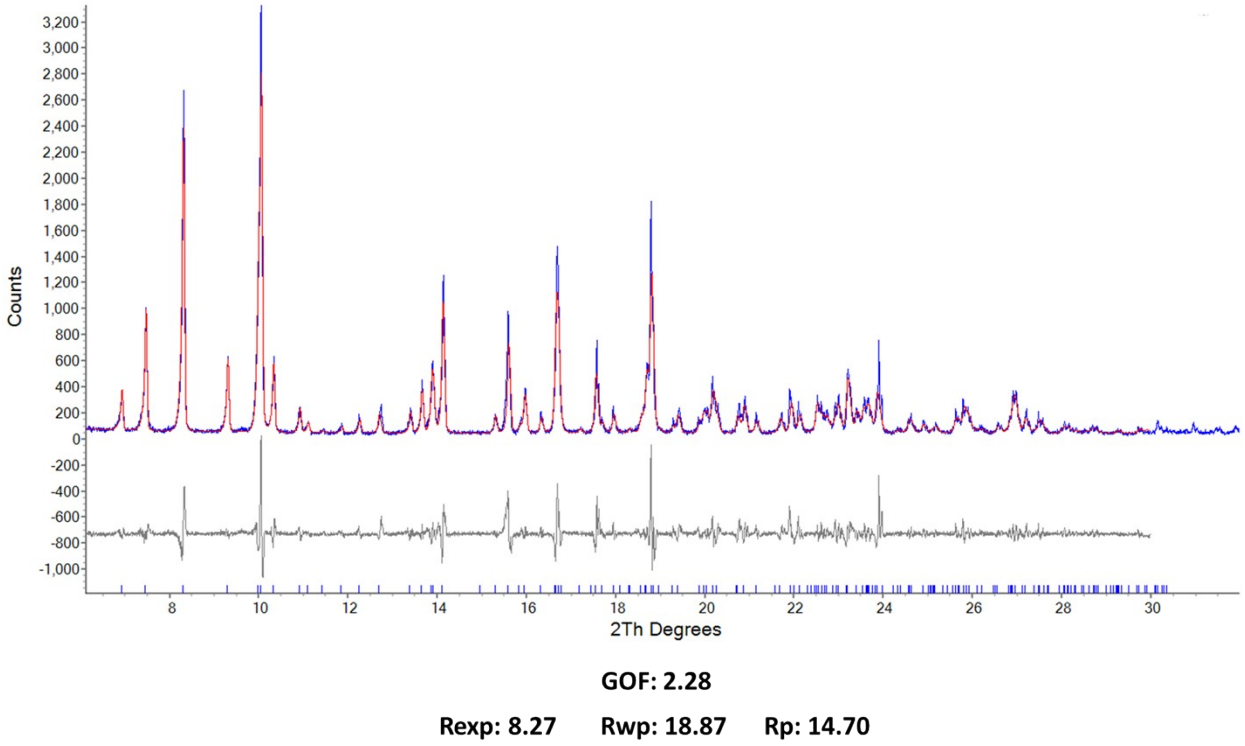

Fig. S1. Rietveld fit of 100 K SCXRD data against a room temperature PXRD experiment of **1**. The CIF calculated (red) and experimental (blue) PXRD patterns are shown at the top. The difference plot is shown below in grey. A Cu source (Kα1 at 1.54 Å) was used for this measurement.

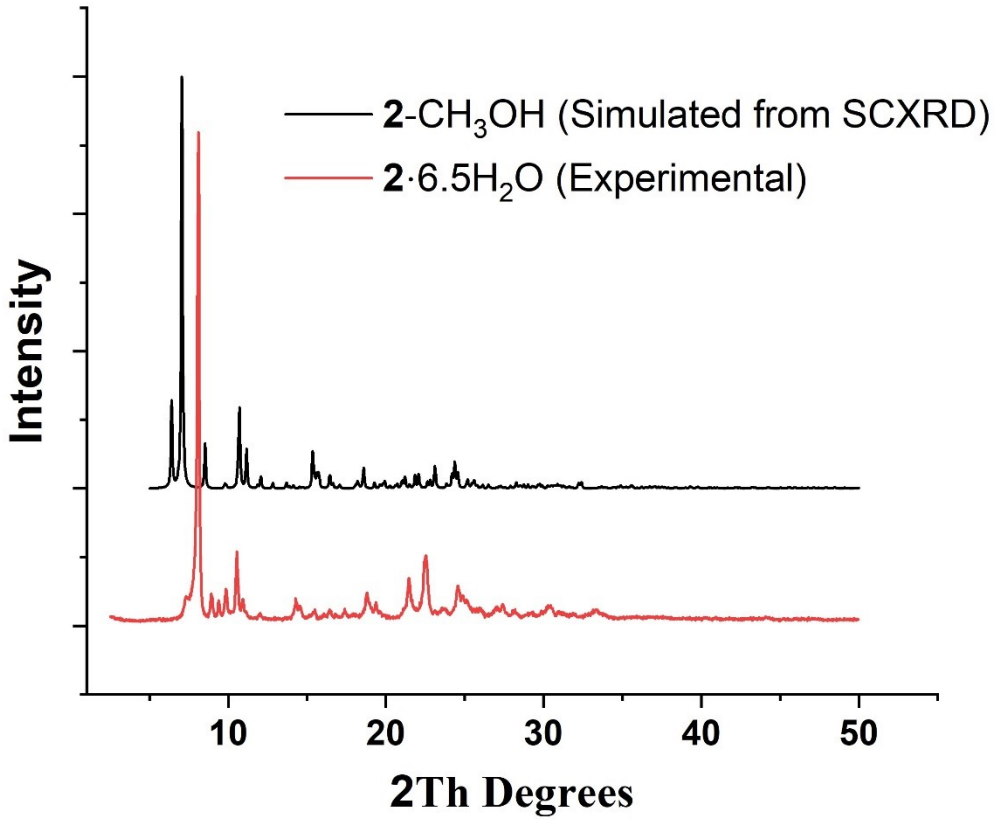

Fig. S2. An overlay of the simulated pattern of **2**-CH_3OH (black) and experimental (red) powder pattern for **2**·$6.5H_2O$. A Cu source (Kα1 at 1.54 Å) was used for this measurement and the simulated diffraction pattern was calculated using the Cu Kα1 wavelength.

S2. Mass spectrometry

High resolution electrospray ionisation mass spectrometry (HR-ESI-MS) indicates that the [Fe**L**]$^{2+}$ cation exists in a solution state. The experimental m/z obtained for [Fe**L**]$^{2+}$ in both compounds (333.6053 m/z) is in good agreement with the calculated m/z = 333.6189 (inset Fig. S1.1 and S1.2) The experimental isotope patterns for all compounds are also in good agreement with the simulated patterns.

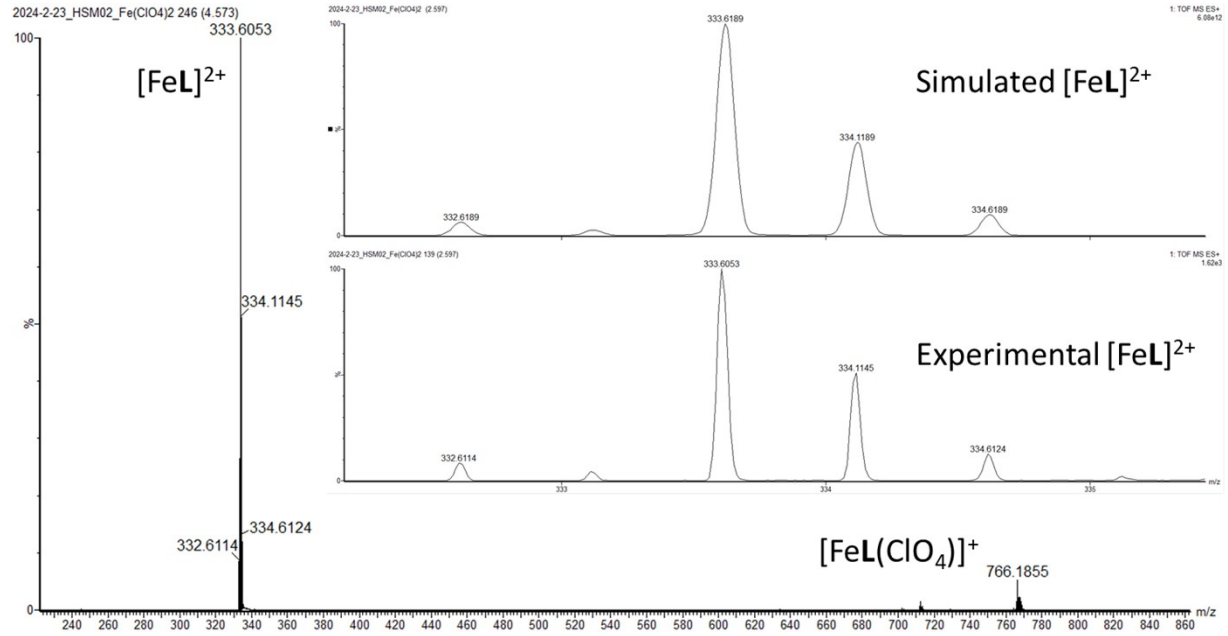

Fig. S3. HR ESI-MS spectrum of **1** in MeCN where the simulated and experimental peaks represent the major species, [Fe**L**]$^{2+}$.

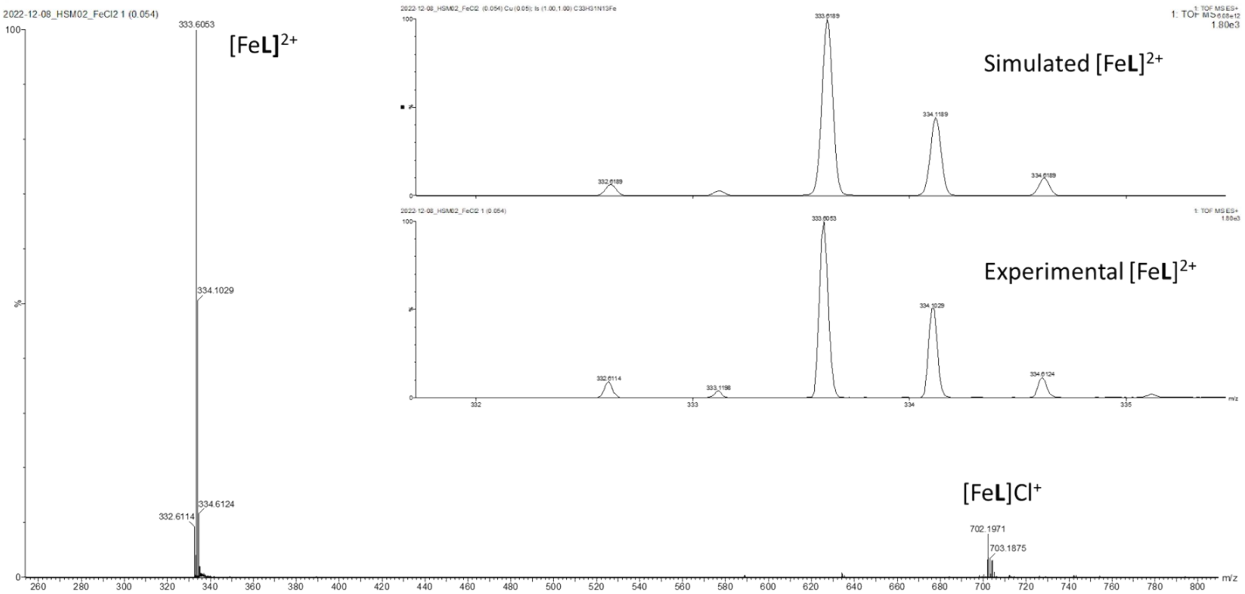

Fig. S4. HR ESI-MS spectrum of **2**·6.5H_2O in CH_3OH where the simulated and experimental peaks represent the major species, [Fe**L**]$^{2+}$.

S3. Scanning electron microscopy - energy dispersive x-ray spectroscopy

Scanning electron microscopy (SEM) portray the rod and plate morphologies and, homogeneity of **1** and **2**·6.5H_2O, respectively. The micrograph of **2**·6.5H_2O show cracking of the crystal from solvent loss. The energy dispersive X-ray spectroscopy (EDS) spectra illustrate that the sample contains the expected elements.

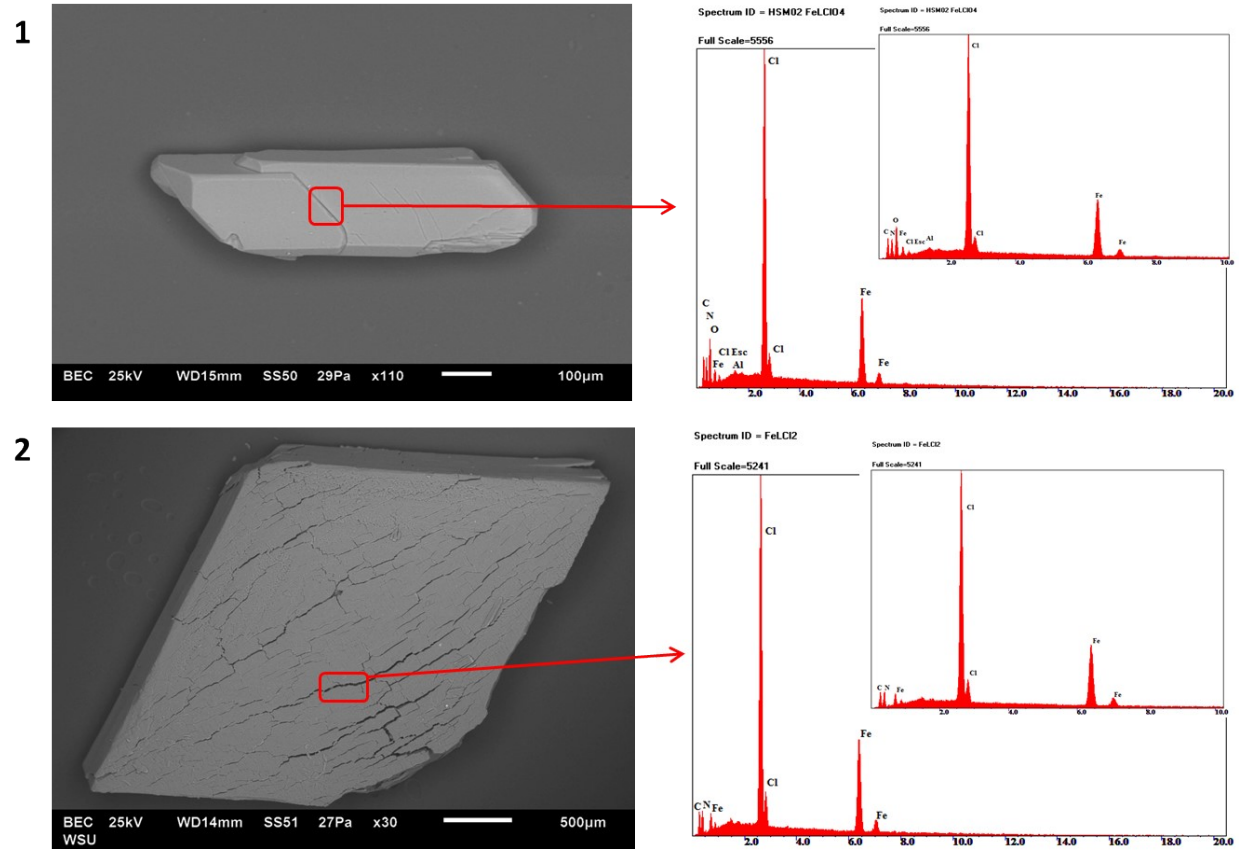

Fig. S5. Backscattering SEM images and corresponding EDS spectrum of **1** and **2**·6.5H_2O.

S4. Simultaneous thermal analysis

Simultaneous thermal analysis (STA) experiments were conducted on **2**·6.5H_2O under argon. The spectrum (Fig. S4.1) indicates two solvent loss events corresponding to a mass loss of 5.38% and 2.07%, totalling 7.45%.

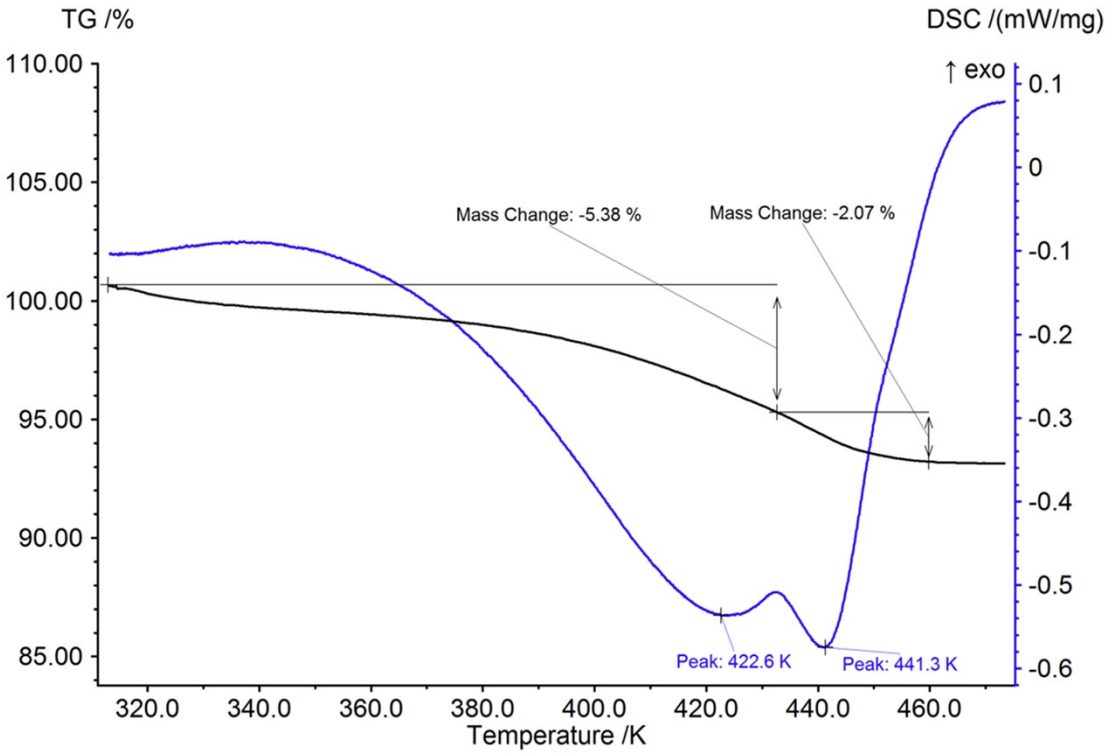

Fig. S6. STA plot of **2**·6.5H_2O showing solvent loss events and corresponding loss of mass.

S5. Magnetic measurements

Magnetic measurements at 1 and 4 K min^{-1} shows scan rate dependency affecting the residual magnetic susceptibility (Fig. S5.1). LIESST experiments have revealed that **2**·$6H_2O$ undergoes a photomagnetic response to green (532 nm) and red (800 nm) light sources (Fig. S5.4).

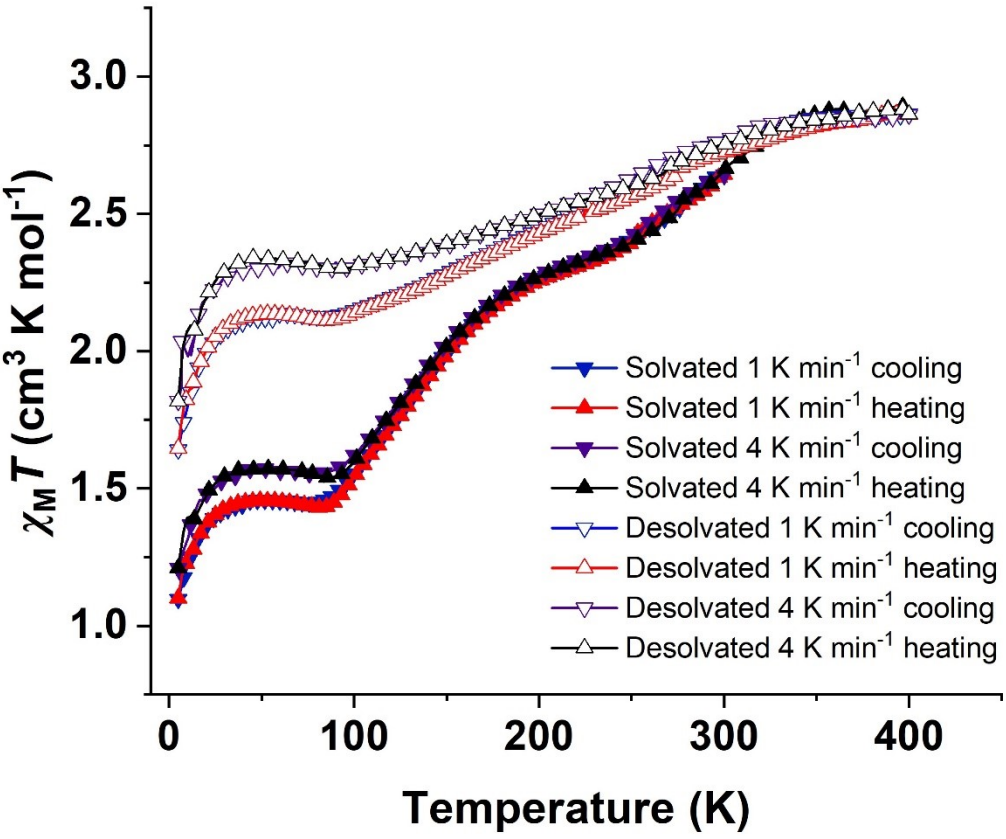

Fig. S7. Magnetic susceptibility plot showing all cooling and heating scans of **2**.

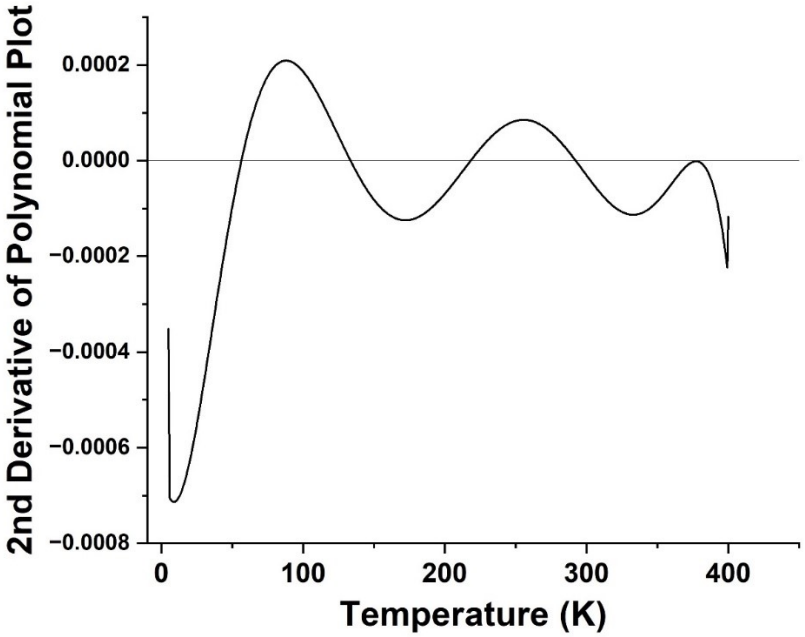

Fig. S8. Second derivative plot of the polynomial curve to calculate T_{SCO} for **2**·6.5H_2O.

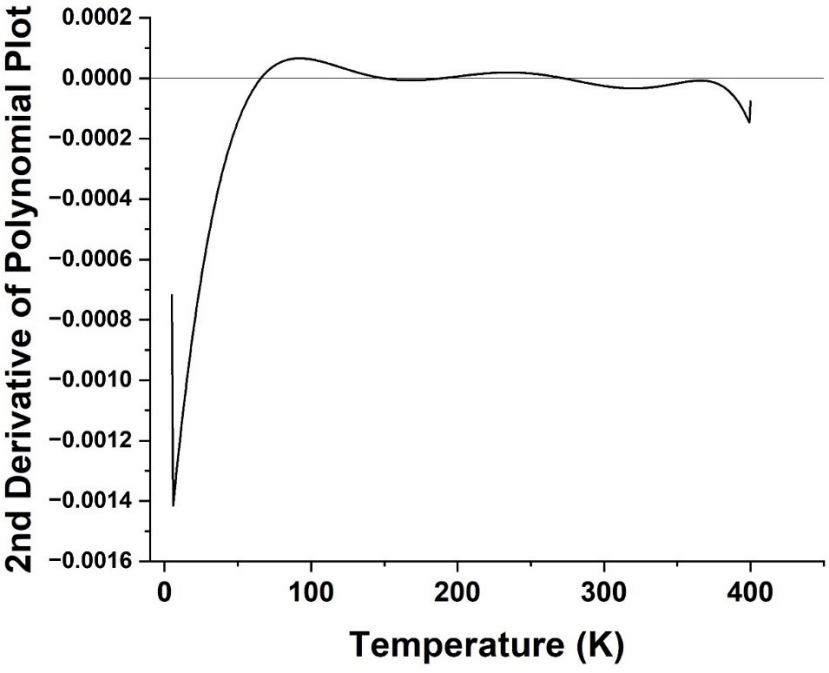

Fig. S9. Second derivative plot of the polynomial curve to calculate T_{SCO} for desolvated **2**.

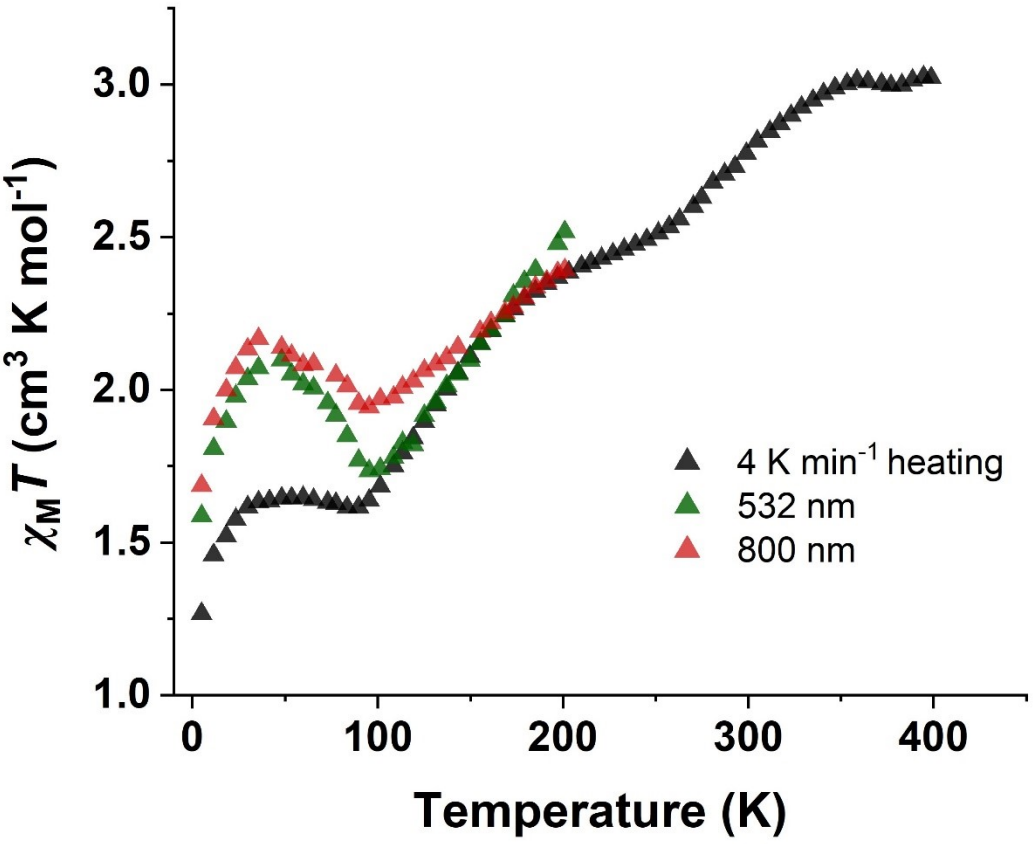

Fig. S10. LIESST plot of **2**·6.5H_2O when exposed to red (800 nm) and green (532 nm) wavelengths.

S6. Solvent masking

The masked electron density at 100 K was attributed to a water molecule in an occupancy of 0.8. The degree of solvation at 100 K was used as a benchmark to inform the solvent mask content at higher temperatures where thermal motion prevented satisfactory modelling of solvent molecules. This means that the degree of solvation in all structures is consistent, and gave a reasonable fit for all structures except for that collected at 200 K.

Table S1. Solvent masking information for VT-SCXRD experiments on single crystals of **2**-CH_3OH.

Temperature (K)	100	150	200	250	300
V (Å^3)	28	29	72	79	219
calculated e^-	**8**	**10**	**20**	**22**	**52**
V/e^-	**3.3**	**2.9**	**3.6**	**3.5**	**4.3**
V/at.	**35**	**29.9**	**55.0**	**29.3**	**36.2**
Content/Formula Unit	0.8 H_2O	0.97 H_2O	1.3 H_2O	0.7 CH_3OH, 1.3 H_2O	2.25 CH_3OH, 1.55 H_2O
assigned e^-	**8**	**10**	**13**	**26**	**56**
m	4	4	4	4	4

S7. Crystallographic data table

Table S2. Crystallographic Data Table for **1**, **2**-CH_3OH and [Fe**L**]$(BF_4)_2$.

Compound	[Fe**L**]$(BF_4)_2$*	**1**	**2**-CH_3OH				
Temperature (K)	**100**	**100**	**100**	**150**	**200**	**250**	**300**
CCDC Number	2170063	2338627	2338626	2338622	2338624	2338625	2338623
Empirical formula	$C_{34}H_{37}B_2F_8FeN_{13}O$	$C_{34}H_{37}Cl_2FeN_{13}O_9$	$C_{36}H_{42.6}Cl_2FeN_{13}O_{5.3}$	$C_{36}H_{46.94}Cl_2FeN_{13}O_{5.3}$	$C_{36}H_{43.6}Cl_2FeN_{13}O_{5.3}$	$C_{36}H_{40.4}Cl_2FeN_{13}O_{5.3}$	$C_{36}H_{45.1}Cl_2FeN_{13}O_{5.3}$
Formula weight	873.23	898.51	868.98	873.40	869.99	866.76	871.50
Temperature/ K	100.0	100	100.00	150.00	200.00	250.00	300.00
Crystal system	monoclinic	monoclinic	monoclinic	monoclinic	monoclinic	monoclinic	monoclinic
Space group	$P2_1/c$	$P2_1/c$	C2/c	C2/c	C2/c	C2/c	C2/c
a/Å	11.565(2)	11.651(2)	32.168(6)	32.213(6)	32.341(7)	32.450(7)	32.281(7)
b/Å	15.555(3)	15.699(3)	16.288(3)	16.294(3)	16.381(3)	16.530(3)	16.537(3)
c/Å	21.169(4)	21.229(4)	20.562(4)	20.582(4)	20.675(4)	20.800(4)	20.748(4)
α/°	90	90	90	90	90	90	90
β/°	91.87(3)	92.15(3)	129.70(3)	129.69(3)	129.70(3)	129.57(3)	129.08(3)

γ/°	90	90	90	90	90	90	90
Volume/Å^3	3806.1(13)	3880.2(13)	8289(4)	8313(4)	8427(4)	8601(4)	8598(4)
Z	4	4	8	8	8	8	8
ρ_{calc}g/cm^3	1.524	1.538	1.393	1.396	1.371	1.339	1.347
μ/mm^{-1}	0.485	0.599	0.551	0.550	0.542	0.531	0.532
F(000)	1792.0	1856.0	3616.0	3651.0	3624.0	3598.0	3636.0
Crystal size/mm^3	0.02 × 0.02 × 0.01	0.1 × 0.1 × 0.1	0.2 × 0.1 × 0.1	0.2 × 0.1 × 0.1	0.2 × 0.1 × 0.1	0.2 × 0.1 × 0.1	0.2 × 0.1 × 0.1
Radiation	MoKα (λ = 0.71073)	MoKα (λ = 0.71073)	MoKα (λ = 0.71073)	MoKα (λ = 0.71073)	MoKα (λ = 0.71073)	MoKα (λ = 0.71073)	MoKα (λ = 0.71073)
2Θ range for data collection/°	3.25 to 57.062	3.228 to 48.812	2.994 to 57.458	2.992 to 57.406	2.976 to 57.402	2.954 to 57.436	2.95 to 43.932
Index ranges	-12 ≤ h ≤ 12, -18 ≤ k ≤ 18, -24 ≤ l ≤ 24	-12 ≤ h ≤ 12, -18 ≤ k ≤ 18, -24 ≤ l ≤ 24	-42 ≤ h ≤ 42, -20 ≤ k ≤ 21, -24 ≤ l ≤ 23	-37 ≤ h ≤ 37, -18 ≤ k ≤ 18, -25 ≤ l ≤ 25	-40 ≤ h ≤ 40, -18 ≤ k ≤ 18, -26 ≤ l ≤ 26	-40 ≤ h ≤ 40, -19 ≤ k ≤ 18, -26 ≤ l ≤ 26	-33 ≤ h ≤ 33, -17 ≤ k ≤ 17, -21 ≤ l ≤ 21
Reflections collected	47189	41658	51901	52375	53513	54313	29622
Independent reflections	7210 [R_{int} = 0.0239, R_{sigma} = 0.0134]	6076 [R_{int} = 0.0374, R_{sigma} = 0.0226]	8539 [R_{int} = 0.0375, R_{sigma} = 0.0221]	8488 [R_{int} = 0.0269, R_{sigma} = 0.0165]	8626 [R_{int} = 0.0290, R_{sigma} = 0.0180]	8791 [R_{int} = 0.0258, R_{sigma} = 0.0147]	4959 [R_{int} = 0.0285, R_{sigma} = 0.0192]
Data/restraints/parameters	7210/0/534	6076/0/534	8539/14/513	8488/16/525	8626/116/502	8791/157/508	4959/154/464

Goodness-of-fit on F^2	1.040	1.168	1.035	1.061	1.036	1.060	1.081
Final R indexes [I>=2σ (I)]	R_1 = 0.0274, wR_2 = 0.0710	R_1 = 0.0325, wR_2 = 0.0900	R_1 = 0.0599, wR_2 = 0.1712	R_1 = 0.0524, wR_2 = 0.1483	R_1 = 0.0468, wR_2 = 0.1352	R_1 = 0.0552, wR_2 = 0.1772	R_1 = 0.0712, wR_2 = 0.2190
Final R indexes [all data]	R_1 = 0.0277, wR_2 = 0.0712	R_1 = 0.0325, wR_2 = 0.0900	R_1 = 0.0658, wR_2 = 0.1775	R_1 = 0.0531, wR_2 = 0.1490	R_1 = 0.0478, wR_2 = 0.1363	R_1 = 0.0575, wR_2 = 0.1809	R_1 = 0.0822, wR_2 = 0.2375
Largest diff. peak/hole / e $Å^{-3}$	0.57/-0.39	0.49/-0.64	1.19/-0.63	1.89/-1.02	1.12/-0.78	1.06/-0.76	0.57/-0.48

*[Fe**L**]$(BF_4)_2$ has been previously reported by our group, and is included here for structural comparison against the compounds studied in this work.

S8. Intermolecular interactions

Table S3. Intermolecular interactions in **1** at 100 K (where all O atoms are part of a ClO_4^- counter-anion)

D-H···A	H···A	D···A	D-H	∠DHA (°)	Symmetry codes to generate D-H atoms
C(11A)-H(11A)···O(2)	2.437	3.195	0.95	136.56	1 - X, -1/2 + Y, 3/2 - Z
C(3B)-H(3B)···O(2)	2.818	3.369	0.95	117.87	1 - X, -1/2 + Y, 3/2 - Z
C(2C)-H(2CB)···O(2)	4.267	4.879	0.99	123.12	-1 + X, Y, Z
C(3C)-H(3C)···O(2)	2.491	3.234	0.95	135.04	-1 + X, Y, Z
C(5C)-H(5C)···O(2)	2.452	3.175	0.95	132.79	-1 + X, Y, Z
C(2A)-H(2AA)···O(3)	2.482	3.433	0.99	160.97	1 - X, 1/2 + Y, 3/2 - Z
C(1A)-H(1AB)···O(4)	3.515	3.995	0.99	112.12	1 - X, 1/2 + Y, 3/2 - Z
C(2A)-H(2AA)···O(4)	2.787	3.628	0.99	143.1	1 - X, 1/2 + Y, 3/2 - Z
C(1B)-H(1BA)···O(4)	2.756	3.746	0.99	177.12	1 - X, 1/2 + Y, 3/2 - Z
C(5C)-H(5C)···O(4)	2.466	3.385	0.95	162.64	-1 + X, Y, Z
C(10C)-H(10C)···O(4)	2.502	3.4	0.95	157.81	-1 + X, Y, Z
C(6B)-H(6B)···O(5)	2.262	3.201	0.95	169.52	-
C(8B)-H(8B)···O(5)	2.457	3.376	0.95	162.88	-
C(6A)-H(6A)···O(6)	2.526	3.412	0.95	155.27	-
C(8A)-H(8A)···O(6)	2.495	3.356	0.95	150.6	-
C(1B)-H(1BB)···O(6)	2.712	3.701	0.99	176.8	2 - X, 1/2 + Y, 3/2 - Z
C(11B)-H(11B)···O(6)	2.427	3.37	0.95	171.7	1 - X, -Y, 1 - Z
C(1A)-H(1AA)···O(7)	2.697	3.369	0.99	125.44	X, 1/2 - Y, -1/2 + Z
C(2A)-H(2AB)···O(7)	2.716	3.342	0.99	121.46	X, 1/2 - Y, -1/2 + Z
C(3A)-H(3A)···O(7)	2.874	3.455	0.95	120.5	X, 1/2 - Y, -1/2 + Z
C(7A)-H(7A)···O(7)	2.486	3.103	0.95	122.56	-
C(8A)-H(8A)···O(7)	2.591	3.132	0.95	116.44	-
C(1A)-H(1AA)···O(8)	2.481	3.469	0.99	175.81	X, 1/2 - Y, -1/2 + Z
C(1B)-H(1BB)···O(8)	2.784	3.483	0.99	128.08	2 - X, 1/2 + Y, 3/2 - Z

C(1C)-H(1CB)···O(8)	2.674	3.35	0.99	125.74	X, 1/2 - Y, -1/2 + Z
C(2C)-H(2CA)···O(8)	2.626	3.477	0.99	144.17	X, 1/2 - Y, -1/2 + Z
C(10B)-H(10B)···O(9)	3.166	3.462	0.95	100.11	1 - X, -Y, 1 - Z
C(11B)-H(11B)···O(9)	2.542	3.155	0.95	122.39	1 - X, -Y, 1 - Z
C(6C)-H(6C)···N(4B)	2.555	3.402	0.95	148.67	1 - X, -Y, 1 - Z
C(8C)-H(8C)···N(4B)	2.455	3.394	0.95	169.62	1 - X, -Y, 1 - Z

Table S4. Intermolecular interactions in **2**-CH_3OH at 100 K

D-H···A	**H···A**	**D···A**	**D-H**	**∠DHA (°)**	**Symmetry codes to generate D-H atoms**
C(6A)-H(6A)···Cl(1)	2.51	3.45	0.95	173.9	-
C(8A)-H(8A)···Cl(1)	2.82	3.67	0.95	141.3	-
C(5B)-H(5B)···Cl(1)	2.49	3.41	0.95	164.6	3/2 - X, 1/2 - Y, 1 - Z
C(10B)-H(10B)···Cl(1)	2.73	3.68	0.95	175.8	3/2 - X, 1/2 - Y, 1 - Z
C(5C)-H(5C)···Cl(1)	2.68	3.63	0.95	171.3	X, 1 - Y, 1/2 + Z
C(10C)-H(10C)···Cl(1)	2.68	3.63	0.95	174.3	X, 1 - Y, 1/2 + Z
C(5A)-H(5A)···Cl(2)	2.45	3.36	0.95	161.2	3/2 -X, 3/2 - Y, 1 - Z
C(10A)-H(10A)···Cl(2)	3.20	4.08	0.95	155.2	3/2 -X, 3/2 - Y, 1 - Z
C(6C)-H(6C)···Cl(2)	2.64	3.57	0.95	168.7	-
C(8C)-H(8C)···Cl(2)	2.61	3.56	0.95	176.8	-
C(7B)-H(7B)···N(4C)	2.58	3.51	0.95	166.1	1 - X, 1 - Y, - Z

Table S5. Intermolecular interactions in **2**-CH_3OH at 150 K

D-H···A	**H···A**	**D···A**	**D-H**	**∠DHA (°)**	**Symmetry codes to generate D-H atoms**
C(6A)-H(6A)···Cl(1)	2.51	3.45	0.95	173.8	-
C(8A)-H(8A)···Cl(1)	2.88	3.67	0.95	141.3	-
C(5B)-H(5B)···Cl(1)	2.49	3.42	0.95	165.0	3/2 - X, 1/2 - Y, 2 - Z
C(10B)-H(10B)···Cl(1)	2.74	3.69	0.95	175.8	3/2 - X, 1/2 - Y, 2 - Z
C(5C)-H(5C)···Cl(1)	2.69	3.63	0.95	171.3	X, 1 - Y, 1/2 + Z

C(10C)-H(10C)···Cl(1)	2.68	3.62	0.95	174.7	X, 1 - Y, 1/2 + Z
C(5A)-H(5A)···Cl(2)	2.45	3.37	0.95	161.0	3/2 -X, 3/2 - Y, 2 - Z
C(10A)-H(10A)···Cl(2)	3.19	4.07	0.95	155.5	3/2 -X, 3/2 - Y, 2 - Z
C(6C)-H(6C)···Cl(2)	2.63	3.57	0.95	168.4	-
C(8C)-H(8C)···Cl(2)	2.61	3.55	0.95	176.0	-
C(7B)-H(7B)···N(4C)	2.59	3.52	0.95	166.8	1 - X, 1 - Y, 1 - Z

Table S6. Intermolecular interactions in **2**-CH_3OH at 200 K

D-H···A	H···A	D···A	D-H	∠DHA (°)	Symmetry codes to generate D-H atoms
C(6A)-H(6A)···Cl(1)	2.52	3.47	0.95	173.7	-
C(8A)-H(8A)···Cl(1)	2.90	3.68	0.95	141.0	-
C(5B)-H(5B)···Cl(1)	2.50	3.43	0.95	165.3	1/2 - X, 3/2 - Y, 1 - Z
C(10B)-H(10B)···Cl(1)	2.75	3.70	0.95	175.4	1/2 - X, 3/2 - Y, 1 - Z
C(5C)-H(5C)···Cl(1)	2.70	3.64	0.95	171.4	X, 1 - Y, 1/2 + Z
C(10C)-H(10C)···Cl(1)	2.70	3.64	0.95	174.3	X, 1 - Y, 1/2 + Z
C(5A)-H(5A)···Cl(2)	2.45	3.36	0.95	160.1	1/2 -X, 1/2 - Y, 1 - Z
C(10A)-H(10A)···Cl(2)	3.18	4.06	0.95	155.4	1/2 -X, 1/2 - Y, 1 - Z
C(6C)-H(6C)···Cl(2)	2.65	3.59	0.95	169.5	-
C(8C)-H(8C)···Cl(2)	2.62	3.56	0.95	176.8	-
C(7B)-H(7B)···N(4C)	2.62	3.55	0.95	168.0	1 - X, 1 - Y, 1 - Z

Table S7. Intermolecular interactions in **2**-CH_3OH at 250 K

D-H···A	H···A	D···A	D-H	∠DHA (°)	Symmetry codes to generate D-H atoms
C(6A)-H(6A)···Cl(1)	2.56	3.49	0.94	174.3	-
C(8A)-H(8A)···Cl(1)	2.95	3.72	0.94	141.0	-
C(5B)-H(5B)···Cl(1)	2.52	3.44	0.94	166.2	1/2 - X, 3/2 - Y, 1 - Z
C(10B)-H(10B)···Cl(1)	2.78	3.71	0.94	173.3	1/2 - X, 3/2 - Y, 1 - Z
C(5C)-H(5C)···Cl(1)	2.70	3.64	0.94	173.0	X, 1 - Y, 1/2 + Z

C(10C)-H(10C)···Cl(1)	2.77	3.71	0.94	175.0	X, 1 - Y, 1/2 + Z
C(5A)-H(5A)···Cl(2)	2.46	3.36	0.94	160.0	1/2 -X, 1/2 - Y, 1 - Z
C(10A)-H(10A)···Cl(2)	3.18	4.05	0.94	155.5	1/2 -X, 1/2 - Y, 1 - Z
C(6C)-H(6C)···Cl(2)	2.66	3.59	0.94	170.6	-
C(8C)-H(8C)···Cl(2)	2.64	3.58	0.94	176.6	-
C(7B)-H(7B)···N(4C)	2.64	3.57	0.94	170.5	1 - X, 1 - Y, 1 - Z

Table S8. Intermolecular interactions in **2**-CH_3OH at 300 K

D-H···A	**H···A**	**D···A**	**D-H**	**∠DHA (°)**	**Symmetry codes to generate D-H atoms**
C(6A)-H(6A)···Cl(1)	2.59	3.52	0.93	176.3	-
C(8A)-H(8A)···Cl(1)	2.99	3.78	0.93	142.4	-
C(5B)-H(5B)···Cl(1)	2.50	3.42	0.93	169.3	1/2 - X, 1/2 - Y, 1 - Z
C(10B)-H(10B)···Cl(1)	2.87	3.80	0.93	171.9	1/2 - X, 1/2 - Y, 1 - Z
C(5C)-H(5C)···Cl(1)	2.70	3.63	0.93	174.7	X, 1 - Y, 1/2 + Z
C(10C)-H(10C)···Cl(1)	2.79	3.72	0.93	178.1	X, 1 - Y, 1/2 + Z
C(5A)-H(5A)···Cl(2)	2.46	3.34	0.93	159.0	1/2 -X, 3/2 - Y, 1 - Z
C(10A)-H(10A)···Cl(2)	3.32	4.18	0.93	154.5	1/2 -X, 3/2 - Y, 1 - Z
C(6C)-H(6C)···Cl(2)	2.68	3.61	0.93	172.7	-
C(8C)-H(8C)···Cl(2)	2.63	3.56	0.93	175.0	-
C(7B)-H(7B)···N(4C)	2.64	3.55	0.93	165.1	1 - X, 1 - Y, 1 - Z

S9. Mutual bonding angles

To quantify the conformational changes of these coordination complexes, the mutual secondary bonding angle was measured. The mutual secondary bonding angle describes the angles between the three ligand arms and depicts the amount of spread occurring at the terminal pyridine groups. In Olex2[1], in each ligand arm a bond was added between the pyridyl group nitrogen and the carbon opposite the same ring (Fig. S10.1). These vectors were taken to represent the vector of the secondary bonding direction of this metalloligand, and the angles between these vectors were measured directly in the GUI.

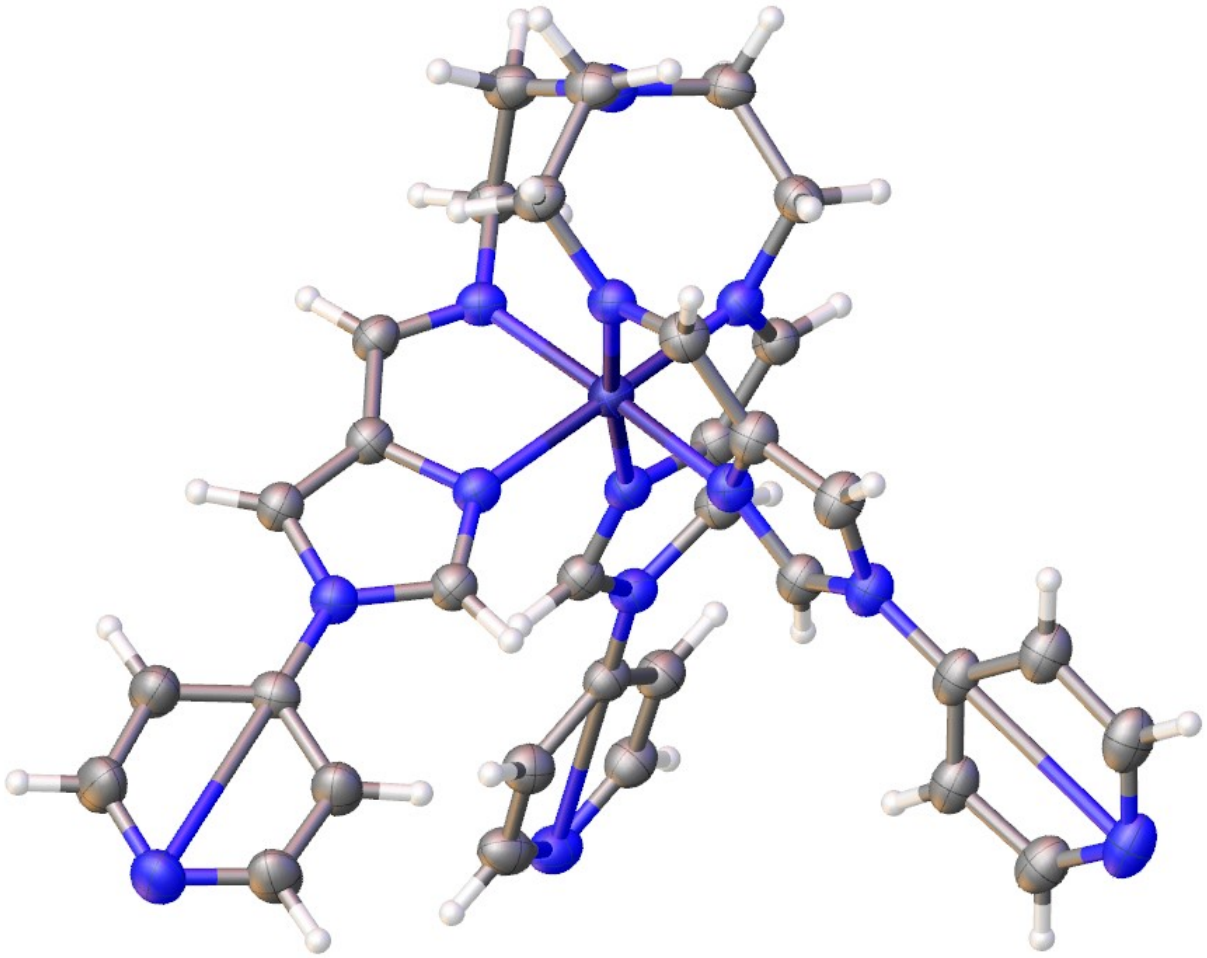

Fig. S11. Illustration showing the calculation of the secondary bonding axis where C-N bonds were added to the terminal pyridyl groups in Olex2.[1]

Table S9. Mutual bonding axes measurements on **1**, **2**-CH_3OH and [Fe**L**]$(BF_4)_2$.

	[Fe**L**]$(BF_4)_2$	**1**	**2**-CH_3OH				
Temperature (K)	100	100	100	150	200	250	300
A|B (°)	57.9	57.776	79.207	79.124	78.921	78.461	76.32
B|C (°)	55.8	56.091	73.712	73.577	73.76	74.282	74.232
A|C (°)	52.2	53.529	74.654	74.65	74.95	74.864	72.082
Average (°)	55.3	55.799	75.858	75.784	75.877	75.869	74.211

S10. References

1 O. V. Dolomanov, L. J. Bourhis, R. J. Gildea, J. A. K. Howard and H. Puschmann, *J. Appl. Cryst.*, 2009, **42**, 339-341.